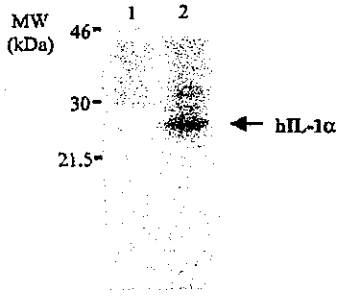

FIGURE 3. Immunoprecipitation of hIL-1α isolated from synoviocyte membrane fraction. Cultured synoviocytes were labeled with [^{35}S]methionine/cysteine (40 μCi/ml) for 6 h. Membrane fraction was obtained as indicated in *Materials and Methods*, followed by immunoprecipitation using anti-hIL-1α polyclonal Ab. *Lane 1*, Immunoprecipitation in the presence of excess unlabeled recombinant hIL-1α. *Lane 2*, immunoprecipitation of synoviocyte membrane fraction, showing the 25-kDa precursor form of hIL-1α (arrow).

effect (data not shown). This indicates that transgene-derived hIL-1α actually localizes within the membrane of synoviocytes.

MA-IL-1 on the surface of synoviocytes is biologically active and promotes synoviocyte proliferation

Kaye and co-workers (31, 32) have reported a IL-1-sensitive T cell clone, D10.G4.1, that can be used to detect and titrate IL-1 by adding test molecules together with Con A. Using these characteristics of D10 cells, MA-IL-1 expression on LPS-stimulated macrophages has been elucidated by [^{3}H]thymidine incorporation into D10 cells cultured on PFA-fixed macrophages (14). This procedure was used to determine the MA-IL-1 activity of synoviocytes from Tg mice. Tg mouse-derived synoviocytes significantly stimulated D10 cell proliferation compared with littermate-derived synoviocytes (Fig. 4*A*). To exclude the possibility of the mitogenic activity of MA-IL-1 actually being attributable to minor contaminants in preparations, neutralizing Ab against hIL-1α/mIL-1α was added to cultures during the assay. Addition of anti-hIL-1α Ab resulted in significant inhibition of D10 cell proliferation, suggesting that bioactivity of synoviocytes is due to transgene-derived MA-IL-1. Furthermore, anti-mIL-1α Ab inhibited D10 cell proliferation to a similar degree as anti-hIL-1α Ab, with inhibition reaching a maximum with the combination of both Abs. Transgene-derived MA-IL-1 thus induces the production of endogenous mouse MA-IL-1, and both forms of MA-IL-1 may play a role in the development of proliferative synovitis in Tg mice. As IL-1 has been shown to act as a mitogen for synoviocytes (33–35), the effects of MA-IL-1 on synoviocyte proliferation were examined. In this experiment, live synoviocytes isolated from Tg mice and RA patients were used as indicator cells for IL-1 activity, instead of D10 cells. Notably, putative MA-IL-1 in Tg mouse-derived synoviocytes led to significant stimulation of [^{3}H]thymidine incorporation into indicator cells compared with that in littermate-derived synoviocytes (Fig. 4*B*), indicating that MA-IL-1 on Tg mouse-derived synoviocytes stimulates synoviocyte self-proliferation via juxtacrine mechanisms.

MA-IL-1 expression and its activity affect severity of arthritis in Tg mice

To elucidate the contribution of MA-IL-1 to the development of arthritis, the severity of arthritis was evaluated according to a scoring system. Clinical symptoms of arthritis in all four paws and histology of bilateral knee joints were scored, and these macroscopic and histological scores were compared between the two Tg mouse lines, Tg1706 and Tg101, which overexpress pro-IL-1α and mature IL-1α, respectively. Interestingly, these scores of Tg1706

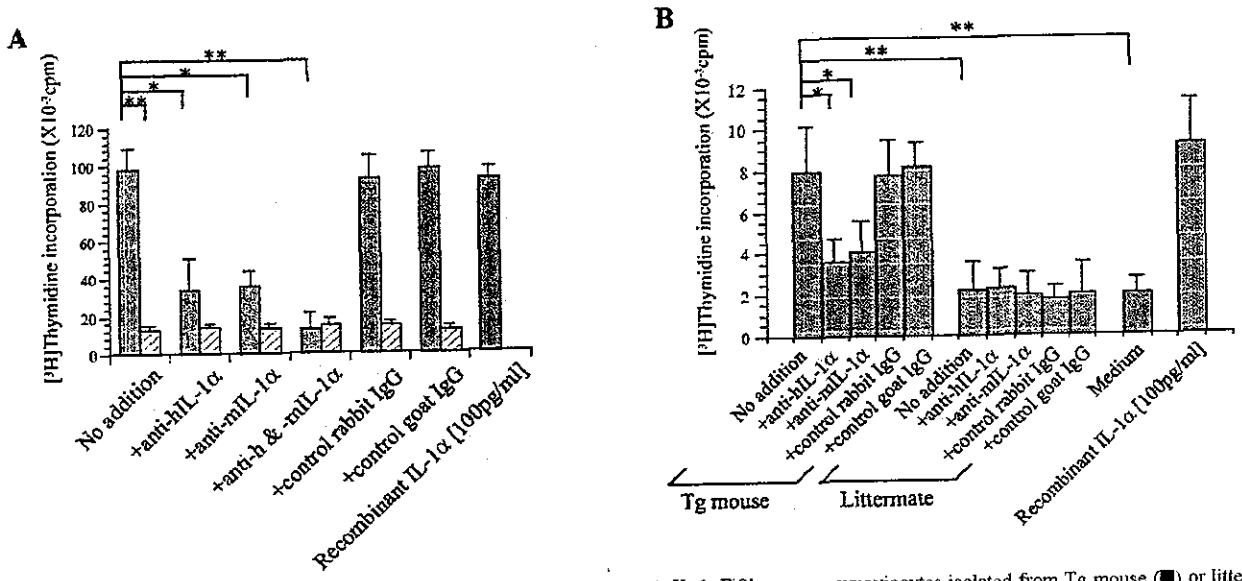

FIGURE 4. *A*, Tg mouse-derived synoviocytes express biologically active MA-IL-1. Fifth-passage synoviocytes isolated from Tg mouse (■) or littermates (▨) were inoculated on 96-well plates and fixed with 1% PFA in PBS for 144 h. D10 cells were distributed to wells and incubated with or without neutralizing Abs against hIL-1α/mIL-1α. Isotype-matched control IgGs were used to exclude a possibility that these neutralizations include nonspecific reactions. [^{3}H]thymidine incorporation into D10 cells was measured during the final 4 h of a 48-h incubation. Data represent the mean counts per minute ± SEM of four separate experiments. *B*, MA-IL-1 contributes to self-proliferation of synoviocytes. Tg mouse- or littermate-derived synoviocytes cultured on 96-well plates were fixed with 1% PFA for 144 h. Live synoviocytes from Tg mouse were overlaid on the fixed cells with or without neutralizing Abs against hIL-1α/mIL-1α. [^{3}H]thymidine incorporation into overlaid synoviocytes was measured during the final 4 h of a 48-h incubation. Control comprised [^{3}H]thymidine incorporation into synoviocytes incubated with medium alone. Data represent the mean counts per minute ± SEM of four separate experiments. *, $p < 0.05$; **, $p < 0.01$

were significantly higher than those of Tg101, indicating relatively severe arthritic phenotype in Tg1706 compared with Tg101 (Fig. 5*A*). In the next experiment, the relationship between MA-IL-1 activity of synoviocytes and severity of arthritis was examined in 10 6-wk-old Tg mice. Correlations between these scores and levels of MA-IL-1, soluble IL-1, and serum hIL-1α were determined. Linear analyses revealed that MA-IL-1 activity displayed significant correlations with both macroscopic and histological scores (Fig. 5*B*). However, soluble IL-1 activity and serum concentrations of hIL-1α displayed no correlation with either score. MA-IL-1 expression in synovial tissue may therefore represent a key element in the development of synovitis and subsequent joint destruction in Tg mice.

Direct cell-to-cell contact is indispensable in promotion of MA-IL-1 activity

To investigate whether direct cell-to-cell interactions are required for MA-IL-1 activity, a coculture system using the cell culture insert with 1-μm pores was employed, allowing the infiltration of macromolecules, but not direct cell-to-cell contact. Similar to the experiment in Fig. 5*B*, live synoviocytes were used as indicator cells for IL-1 activity and cocultured with PFA-fixed synoviocytes with or without cell culture inserts. Significant differences in live synoviocyte proliferation were observed between the two different cultures. Live synoviocytes displayed obvious proliferation when directly cultured with PFA-fixed synoviocytes without separation (Fig. 6). However, once cells were separated from each other using a cell culture insert, the proliferative activity of PFA-fixed synoviocytes was abrogated. When neutralizing Abs against hIL-1α/mIL-1α were added to cultures during the assay, synoviocyte proliferation was significantly diminished in culture *without* cell culture insert, indicating that this proliferative activity was attributable to MA-IL-1 in PFA-fixed synoviocytes. Weak, but nonsignificant, neutralization was observed in culture with the cell culture insert; in contrast to D10 cells, Tg mouse-derived synoviocytes spontaneously produce soluble IL-1 and MA-IL-1, and endogenous IL-1-dependent proliferation of these cells was blocked by the specific Abs. These results indicate that direct cell-to-cell contact is indispensable in the promotion of proliferative activity by MA-IL-1.

Differential kinetics between synthesis of MA-IL-1 and soluble IL-1

To investigate the kinetics of synthesis for MA-IL-1 and soluble IL-1, incorporation of [^{3}H]thymidine into synoviocytes was determined when cells were overlaid on PFA-fixed synoviocytes as a

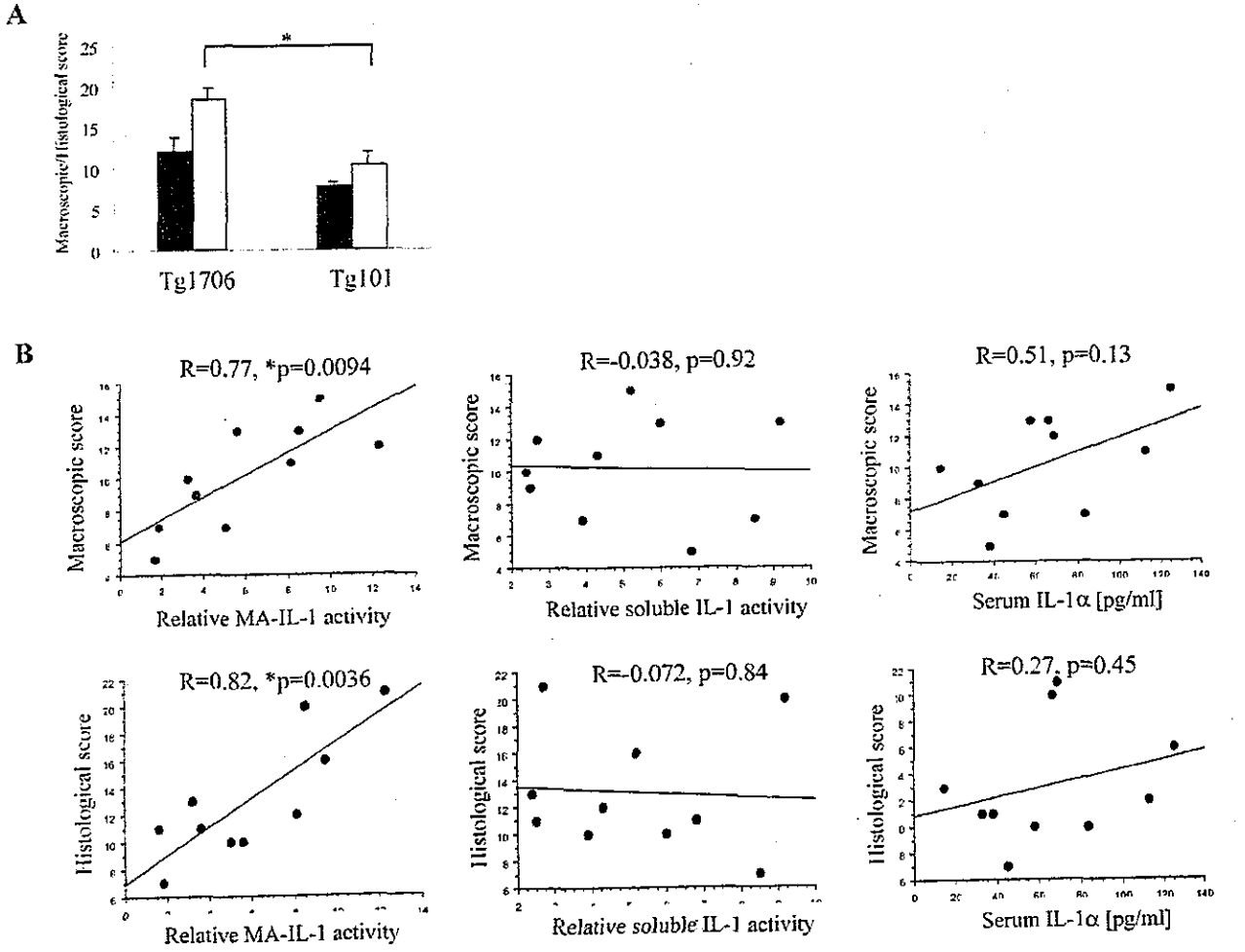

FIGURE 5. *A*, Comparison of severity of arthritis between Tg1706 and Tg101. Macroscopic and histological findings were scored at 6-wk-old Tg mice. Data are presented as the mean + SEM of four mice. *B*, Correlation between macroscopic score, histological score, relative MA-IL-1 activity, relative soluble IL-1 activity, and serum hIL-1α level in 10 6-wk-old Tg mice. Data are presented as the coefficient (R) and p value derived from linear regression analysis. *, $p < 0.05$.

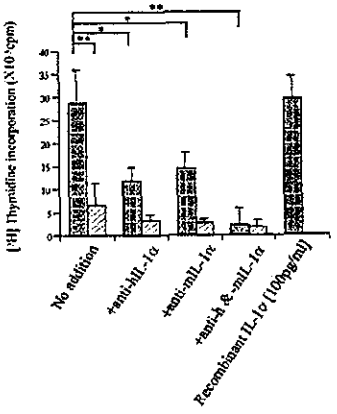

FIGURE 6. MA-IL-1 promotes synoviocyte proliferation in a cell-to-cell contact-dependent manner. Tg mouse-derived synoviocytes cultured on 24-well plates were fixed with 1% PFA for 144 h. Live synoviocytes were added directly to the fixed synoviocytes (■) or the top compartment of the cell culture insert (▨) and incubated for 48 h. For blockade of IL-1 activity, neutralizing Abs against hIL-1α/mIL-1α were added during incubation. [³H]Thymidine incorporation into live synoviocytes was determined during the final 4 h of a 48-h incubation. Data are presented as the mean counts per minute ± SEM for four separate experiments. *, $p < 0.05$; **, $p < 0.01$

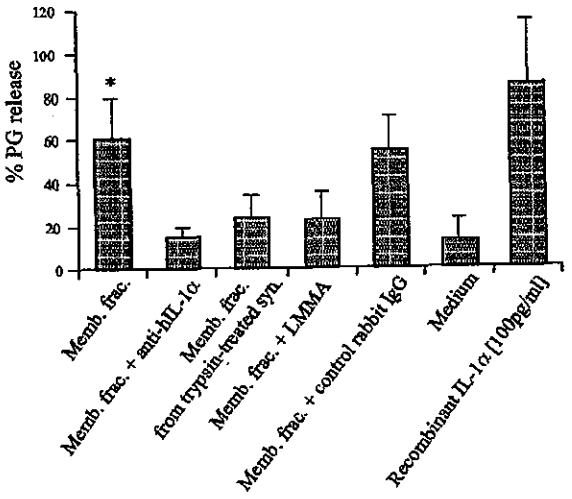

FIGURE 8. MA-IL-1 stimulates PG release from cartilage matrix through generation of NO. Cultured articular chondrocytes were radiolabeled with [^{35}S]sulfate for 24 h, then incubated for 48 h with synoviocyte membrane fraction alone, membrane fraction plus anti hIL-1α Ab, membrane fraction plus 100 mM LMMA, or membrane fraction isolated from trypsin-treated synoviocytes. Control data were derived from chondrocytes without membrane fraction. The release of ^{35}S-labeled PG from the cell and matrix layer to culture supernatant was examined. The percent PG release was calculated according to the following equation: % release = [^{35}S]PG in supernatant/[^{35}S]PG in cell and matrix + [^{35}S]PG in supernatant. Data are presented as the mean counts per minute ± SEM for four separate experiments. *, $p < 0.05$ compared with the control.

feeder layer of MA-IL-1. Soluble IL-1 secreted into culture supernatant by overlaid synoviocytes was demonstrable from 24 h after inoculation and plateaued between 72 and 96 h (Fig. 7*A*), whereas the corresponding MA-IL-1 activity reached a plateau by 24 h after inoculation, remaining stable until at least 96 h (Fig. 7*B*). In addition, the proliferative activity of soluble IL-1 was ~5-fold higher than that of MA-IL-1.

MA-IL-1 induces PG release from cartilage matrix in vitro

Monolayer-cultured articular chondrocytes derived from Japanese White rabbits were labeled with [^{35}S]sulfate for 24 h, then incubated with synoviocyte membrane fraction in the presence or the absence of anti-hIL-1α Ab for 48 h. Release of ^{35}S-labeled PG from cell and matrix layer was examined. The synoviocyte membrane fraction significantly stimulated PG release into culture supernatant compared with control (Fig. 8), and stimulation was decreased almost to control levels by the addition of anti-IL-1α Ab. In contrast, the membrane fraction isolated from synoviocytes treated with mild trypsin did not affect PG release, compatible with the flow cytometric data in Fig. 3*C* showing that MA-IL-1 has a tryptic cleavage site and can be removed by mild trypsin treatment. Furthermore, the NO synthase inhibitor, LMMA, for the most part inhibited membrane fraction-stimulated PG release, indicating the involvement of NO in this process. These data suggest that MA-IL-1 induces PG release from the cell and matrix through generating NO in chondrocyte monolayer culture, further indicating that MA-IL-1 may play a role in cartilage destruction in vivo.

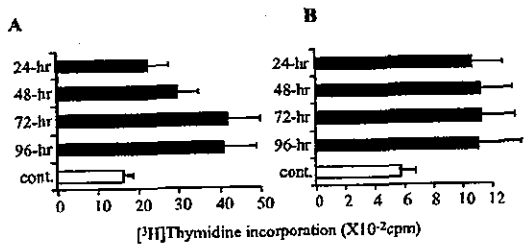

FIGURE 7. Synthetic kinetics of MA-IL-1 and soluble IL-1α. Fifth-passage synoviocytes derived from Tg mice were fixed on the indicated day of culture after inoculation. Corresponding culture supernatants were collected immediately before fixation of synoviocytes. D10 cells were incubated on fixed cells or with a 25% (v/v) final concentration of culture supernatants. The IL-1 activity of supernatants (*A*) and fixed cells (*B*) was determined by measuring [³H]thymidine incorporation into D10 cells during the last 4 h of a 48-h incubation (■). Control data for synoviocytes were derived from littermates (□). Data are presented as the mean counts per minute ± SEM for four separate experiments.

Discussion

MA-IL-1 was found to play key roles in the development of arthritic phenotypes in Tg mice. Of interest is the fact that both macroscopic and histological scores were correlated with activity of MA-IL-1, but not with activity of soluble IL-1 produced by synoviocytes. Moreover, cartilage destruction of Tg101 line overexpressing 17-kDa mature IL-1α was relatively mild even at 12 wk after birth, although the Tg1706 line overexpressing pro-IL-1α demonstrated complete loss of cartilage at 8 wk after birth, which reflected low macroscopic and histological scores in the Tg101 line. This observation was not attributable to the difference in levels of transgene expression between the two lines, because the levels of serum IL-1α were almost similar (~100 pg/ml). Thus, as in Tg mouse studies on membrane-associated TNF (36, 37), the arthritogenic properties of MA-IL-1 may be sufficient to cause severe arthritis even in conditions without processing of proteins to mature form.

However, we cannot neglect the fact that, in general, transgene expression can be affected by copy number and integration site of the transgene, and a simple comparative study of phenotypic characteristics among Tg mouse lines is unlikely to provide informative data. In actual fact, we established two transgenic founders for

each Tg mouse for pro- and active IL-1α. As assessed by tail Southern blot analysis, copy number of transgenes was similar among the four transgenic founders (three or four copies), and differences in integration site were confirmed by fluorescence in situ hybridization analysis. Northern blot analysis revealed quite similar levels and patterns of mRNA expression in all four transgenic founders, and of course in offspring of Tg101 and Tg1706. All four founders exhibited arthritic phenotypes, and a more severe arthritic phenotype in pro-IL-1α Tg mice than in active IL-1α Tg mice was noted as a universal trend, even in offspring. This indicates that in our study the effects of copy number and integration site of transgenes can be neglected, allowing direct comparison of the two Tg mouse lines. We therefore believe that Tg mice for pro-IL-1α exhibited a more progressive arthritic phenotype than mice for active IL-1α, and membrane IL-1 plays an important role in the evolution of inflammatory arthritis.

To date, MA-IL-1 has been shown to be more potent than soluble IL-1 in a variety of situations, such as neutrophil extravasation via endothelial cells, T cell activation during Ag presentation, and osteoclast formation through up-regulation of receptor activator NF-κB ligand expression on osteoblasts, all of which play crucial roles in the development of inflammatory joint diseases. Of the pleiotropic activities of MA-IL-1, the present study focused on the effects on synoviocytes and chondrocytes, as IL-1 has been shown to act as a mitogen for rheumatoid synovial fibroblasts, and abnormal IL-1 production contributes to synovial proliferation and degradation of the cartilage matrix in RA and collagen-induced arthritis in mice. As MA-IL-1 synthesis is spontaneously promoted in hIL-1α Tg mice and persists due to the characteristics of the promoter, synoviocytes cultured on PFA-fixed synoviocytes displayed marked proliferation in the absence of stimuli. Moreover, transgene-derived hIL-1α further up-regulated endogenous mouse MA-IL-1 synthesis via autocrine mechanisms, and this may also be involved in the joint pathology of hIL-1α Tg mice.

Kurt-Jones et al. (12) provided the first evidence that PFA-fixed macrophages stimulate IL-1-sensitive T cell clone, D10 G4.1 proliferation due to IL-1 activity on the external plasma membrane of macrophage. In the present study MA-IL-1 expression on the surface of synoviocytes isolated from arthritic joints was directly identified using flow cytometry. Cellular staining regardless of membrane permeabilization and dissociation of hIL-1α from the cell surface by mild trypsin treatment indicated that IL-1α is undoubtedly associated with the exterior plasma membrane surface of synoviocytes. Matsushima et al. (30) also documented the release of biologically active IL-1 from plasma membrane, when LPS-stimulated macrophages are treated with mild trypsin or plasmin-like proteases.

IL-1α precursor propeptide lacks a classical signal sequence (4), which is known to regulate the processing of secreted and integral plasma membrane-associated proteins. To date, a number of post-translational modifications within the NH_2-terminal domain have been proposed to affect the intracellular distribution of IL-1α, including phosphorylation (5), mannosylation (6), and myristolation (7). However, the details of these processes have remained unknown. Several speculations have been proposed regarding such post-translational modifications and their impact on intracellular distribution of IL-1α. One investigator has demonstrated that phosphorylation of newly synthesized IL-1α signifies intracellular routing of IL-1α precursor, and ~10% of phosphorylated IL-1α precursor is committed to the membrane-associated form. Another study revealed that glycosylation of IL-1α precursor allows association with membrane-bound lectins and membrane-localization of IL-1α (6). Alternatively, striking evidence has been proposed that physical injury or programmed cell death (i.e., apoptosis) play a role in IL-1α secretion through membrane disruption (38). Although certain post-translational modifications are likely to reflect the difference between transgene-predicted (25 kDa) and observed (23 kDa) masses of IL-1α precursor in immunoprecipitation of the synoviocyte membrane fraction in IL-1α Tg mice, the mechanisms affecting membrane localization of IL-1α remain unknown.

MA-IL-1 expression on the surface of synoviocytes was clarified from another perspective. Synoviocytes were plated onto 24-well plates and fixed using 1% PFA. Live synoviocytes were directly added to fixed synoviocytes or the top compartment of the cell culture insert, allowing soluble IL-1α, but not MA-IL-1, to migrate between the top and bottom compartments. This experiment indicated that synoviocytes without separation engaged in direct cell-to-cell interactions, resulting in higher proliferation attributable to the activities of soluble IL-1 plus MA-IL-1. However, the true magnitude of [^{3}H]thymidine incorporation into indicator synoviocytes cultured on the PFA-fixed synoviocytes actually appeared higher than that cultured on nonfixed live synoviocytes. This can be explained by our unpublished observations that live synoviocytes spontaneously produce IL-1 receptor antagonist in vitro, which may block IL-1 activity during the experiment.

As reported by van de Loo et al. (39, 40), IL-1 inhibits synthesis of PG by chondrocytes through generation of NO in zymosan-induced arthritis. The present study demonstrated that membrane fraction isolated from synoviocytes induces PG release from the cartilage matrix in chondrocyte monolayer culture, and that this phenomenon is mediated by NO synthesis. This indicates that MA-IL-1 within the membrane is essentially implicated in chondrocyte PG loss, suggesting the possibility that MA-IL-1 contributes to cartilage destruction during the course of arthritis in IL-1α Tg mice. However, PG loss was not detected when chondrocytes were cultured in agarose gels (data not shown). The absence of chondrocyte PG loss is probably attributable to the prevention of direct cell-to-cell contact by the surrounding agarose gel. Chondrocyte PG loss caused by the synoviocyte membrane fraction may thus, for the most part, be due to MA-IL-1 within the membrane.

Finally, the importance of membrane-associated molecules proposed in the current experimental study is that cell-cell interactions between macrophage-like synoviocytes and T lymphocytes activate the production of proinflammatory cytokines at the inflamed synovium (41–43). These include membrane-associated IL-1 and TNF, which induce fibroblast-like synoviocytes to produce large amounts of matrix metalloproteinases that degrade cartilage and bone. In the present study using IL-1α Tg mice, MA-IL-1 expressed on synoviocytes may trigger synoviocyte self-proliferation and induce cartilage degradation, mechanisms that may operate in the cartilage-pannus junction through cell-cell interactions in vivo. Moreover, a correlation between MA-IL-1 activity and severity of arthritis indicates that MA-IL-1 is a potent effector of joint inflammation. As the present results were obtained purely from animal studies, the importance and extent of MA-IL-1 contribution to the pathogenesis of human inflammatory joint diseases such as RA warrant investigation.

Acknowledgments

We are grateful to the late Prof. Masayuki Shimmei (Department of Orthopedic Surgery, National Defense Medical College) for the planning of this investigation. We also thank Prof. Takushi Tadakuma (Department of Parasitology, National Defense Medical College) for providing the D10.G4.1 cells used in this study.

References

1. Niki, Y., H. Yamada, S. Seki, T. Kikuchi, H. Takaishi, Y. Toyama, K. Fujikawa, and N. Tada. 2001. Macrophage- and neutrophil-dominant arthritis in human IL-1α transgenic mice. *J. Clin. Invest. 107:1127.*

2. March, C. J., B. Mosley, A. Larsen, D. P. Cerretti, G. Braedt, V. Price, S. Gillis, C. S. Henney, S. R. Kronheim, and K. Grabstein. 1985. Cloning, sequence and expression of two distinct human interleukin-1. *Nature 315:641.*
3. Mosley, B., D. L. Urdal, K. S. Prickett, A. Larsen, D. Cosman, P. J. Conlon, S. Gillis, and S. K. Dower. 1987. The interleukin-1 receptor binds to the human interleukin-1α precursor but not the interleukin-1β precursor. *J. Biol. Chem. 262:2941.*
4. Dinarello, C. A. 1996. Biologic basis for interleukin-1 in disease. *Blood 87:2095.*
5. Beuscher, H. U., M. W. Nickells, and H. R. Colten. 1988. The precursor of interleukin-1α is phosphorylated at residue serine 90. *J. Biol. Chem. 263:4023.*
6. Brody, D. T., and S. K. Durum. 1989. Membrane IL-1: IL-1α precursor binds to the plasma membrane via a lectin-like interaction. *J. Immunol. 143:1183.*
7. Stevenson, F. T., S. L. Bursten, C. Fanton, R. M. Locksley, and D. H. Lovett. 1993. The 31-kDa precursor of interleukin-1α is myristolated on specific lysines within the 16-kDa N-terminal propiece. *Proc. Natl. Acad. Sci. USA 90:7245.*
8. Carruth, L., S. Demczuk, and S. Mizel. 1991. Involvement of a calpain-like protease in the processing of the murine interleukin-1α precursor. *J. Biol. Chem. 266:12162.*
9. Kobayashi, Y., K. Yamamoto, T. Saido, H. Kawasaki, and J. J. Oppenheim. 1990. Identification of calcium-activated neutral protease as a processing enzyme of human interleukin 1α. *Proc. Natl. Acad. Sci. USA 87:5548.*
10. Lee, R. T., W. H. Briggs, G. C. Cheng, H. B. Rossiter, P. Libby, and T. Kupper. 1997. Mechanical deformation promotes secretion of IL-1α and IL-1 receptor antagonist. *J. Immunol. 159:5084.*
11. Conlon, P. J., K. H. Grabstein, A. Alpert, K. S. Prickett, T. P. Hopp, and S. Gillis. 1987. Localization of human mononuclear cell interleukin 1. *J. Immunol. 139:98.*
12. Kurt-Jones, E. A., D. I. Beller, S. B. Mizel, and E. R. Unanue. 1985. Identification of a membrane-associated interleukin-1 in macrophages. *Proc. Natl. Acad. Sci. USA 82:1204.*
13. Junming, L. E., D. Weinstein, U. Gubler, and J. Vilcek. 1987. Induction of membrane-associated interleukin 1 by tumor necrosis factor in human fibroblasts. *J. Immunol. 138:2137.*
14. Kurt-Jones, E. A., W. Fiers, and J. S. Pober. 1987. Membrane interleukin 1 induction on human endothelial cells and dermal fibroblasts. *J. Immunol. 139:2317.*
15. Zola, H., L. Flego, Y. T. Wong, P. J. Macardle, and J. S. Kenney. 1993. Direct demonstration membrane IL-1α on the surface on circulating B lymphocytes and monocytes. *J. Immunol. 150:1755.*
16. Yamashita, U., F. Shirakawa, and H. Nakamura. 1987. Production of interleukin 1 by adult T cell leukemia (ATL) cell lines. *J. Immunol. 138:3284.*
17. Acres, R. B., A. L. F. Larsen, and P. J. Conlon. 1987. IL 1 expression in a clone of human T cells. *J. Immunol. 138:2132.*
18. Nishimura, T., Y. Ishihara, T. Noguchi, and T. Koga. 1989. Membrane IL-1 induces bone resorption in organ culture. *J. Immunol. 143:1881.*
19. Kaplanski, G., R. Porat, K. Aiura, J. K. Erban, and C. A. Dinarello. 1993. Activated platelets induce endothelial secretion of interleukin-8 in vitro via an interleukin-1-mediated event. *Blood 81:2492.*
20. Beasley, D., and A. L. Cooper. 1999. Constitutive expression of interleukin-1α precursor promotes human vascular smooth muscle cell proliferation. *Am. J. Physiol. 276:H901.*
21. Weaver, C. T., and E. R. Unanue. 1986. T cell induction of membrane IL-1 on macrophages. *J. Immunol. 137:3868.*
22. Suresh, A., and A. Sodhi. 1991. Production of interleukin-1 and tumor necrosis factor by bone marrow-derived macrophages: effect of cisplatin and lipopolysaccharide. *Immunol. Lett. 30:93.*
23. Nishihara, T., T. Takahashi, Y. Ishihara, H. Senpuku, and T. Koga. 1994. Membrane-associated interleukin-1 promotes osteoclast-like cell formation in vitro. *Bone Miner. 25:15.*
24. McMahon, G. A., S. Garfinkel, I. Prudovsky, X. Hu, and T. Maciag. 1997. Intracellular precursor interleukin (IL)-1α, but not mature IL-1α, is able to regulate human endothelial cell migration in vitro. *J. Biol. Chem. 272:28202.*
25. van den Berg, W. B., L. A. B. Joosten, M. Helsen, and F. A. J. van de Loo. 1994. Amelioration of established murine collagen-induced arthritis with anti-IL-1 treatment. *Clin. Exp. Immunol. 95:237.*
26. Bailly, S., B. Ferrua, M. Fay, and M. A. Gougerot-Pocidalo. 1990. Paraformaldehyde fixation of LPS-stimulated human monocytes: technical parameters permitting the study of membrane IL-1 activity. *Eur. Cytokine Network 1:47.*
27. Maeda, T., K. Balakrishnan, and Q. Mehdi. 1983. A simple and rapid method for the preparation of plasma membranes. *Biochim. Biophys. Acta 731:115.*
28. Helle, M., L. Boeije, and L. A. Aarden. 1988. Functional discrimination between interleukin 6 and interleukin 1. *Eur. J. Immunol. 18:1535.*
29. Masuda, K., H. Shirota, and E. J. M. A. Thonar. 1994. Quantification of ^{35}S-labeled proteoglycans complexed to Alcian Blue by rapid filtration in multiwell plates. *Anal. Biochem. 217:167.*
30. Matsushima, K., M. Taguchi, E. J. Kovacs, H. A. Young, and J. J. Oppenheim. 1986. Intracellular localization of human monocyte associated interleukin 1 (IL 1) activity and release of biologically active IL 1 from monocytes by trypsin and plasmin. *J. Immunol. 136:2883.*
31. Kaye, J., S. Porcelli, J. Tite, B. Jones, and C. A. Janeway, Jr. 1983. Both a monoclonal antibody and antisera specific for determinants unique to individual cloned helper T cell lines can substitute for antigen and antigen-presenting cells in the activation of T cells. *J. Exp. Med. 158:836.*
32. Kaye, J., S. Gillis, S. B. Mizel, E. M. Shevach, T. R. Malek, C. A. Dinarello, L. B. Lachman, and C. A. Janeway, Jr. 1984. Growth of a cloned helper T cell line induced by a monoclonal antibody specific for the antigen receptor: interleukin 1 is required for the expression of receptors for interleukin 2. *J. Immunol. 133:1339.*
33. Rupp, E. A., P. M. Cameron, C. S. Ranawat, J. A. Schmidt, and B. K. Bayne. 1986. Specific bioactivities of monocyte-derived interleukin-1α and interleukin-1β are similar to each other on cultured murine thymocytes and on cultured human connective tissue cells. *J. Clin. Invest. 78:836.*
34. Alvaro-Gracia, J. M., N. J. Zvaifler, and G. S. Firestein. 1990. Cytokines in chronic inflammatory arthritis. V. Mutual antagonism between interferon-gamma and tumor necrosis factor-α on HLA-DR expression, proliferation, collagenase production and granulocyte macrophage colony-stimulating factor production by rheumatoid arthritis synoviocytes. *J. Clin. Invest. 86:1790.*
35. Butler, D. M., D. S. Piccoli, P. H. Hart, and J. A. Hamilton. 1988. Stimulation of human synovial fibroblast DNA synthesis by recombinant human cytokines. *J. Rheumatol. 15:1463.*
36. Probert, L., K. Akassoglou, L. Alexopoulou, E. Douni, S. Haralambous, S. Hill, G. Kassiotis, D. Kontoyiannis, M. Pasparakis, D. Plows, et al. 1996. Dissection of the pathologies induced by transmembrane and wild-type tumor necrosis factor in transgenic mice. *J. Leukocyte Biol. 59:518.*
37. Georgopoulos, S., D. Plows, and G. Kollias. 1996. Transmembrane TNF is sufficient to induce localized tissue toxicity and chronic inflammatory arthritis in transgenic mice. *J. Inflamm. 46:86.*
38. Hogquist, K. A., M. A. Nett, E. R. Unanue, and D. D. Chaplin. 1991. Interleukin 1 is processed and released during apoptosis. *Proc. Natl. Acad. Sci. USA 88:8485.*
39. van de Loo, A. A. J., and W. B. van den Berg. 1990. Effects of murine recombinant IL-1 on synovial joints in mice: quantification of patellar cartilage metabolism and joint inflammation. *Ann. Rheum. Dis. 49:238.*
40. Van de Loo, F. A. J., O. J. Arntz, F. H. J. van Enckevort, P. L. E. M. van Lent, and W. B. van den Berg. 1998. Reduced cartilage proteoglycan loss during zymosan-induced gonarthritis in NOS2-deficient mice and in anti-interleukin-1-treated wild-type mice with unabated joint inflammation. *Arthritis Rheum. 41:634.*
41. Seckinger, P., M. T. Kaufmann, and J. M. Dayer. 1990. An Interleukin 1 inhibitor affects both cell-associated interleukin 1-induced T cell proliferation and PGE_2/collagenase production by human dermal fibroblasts and synovial cells. *Immunobiology 180:316.*
42. Burger, D., R. Rezzonico, H. M. C. Modoux, R. A. Pierce, H. G. Welgus, and J. M. Dayer. 1998. Imbalance between interstitial collagenase and tissue inhibitor of metalloproteinases 1 in synoviocytes and fibroblasts upon direct contact with stimulated T lymphocytes: involvement of membrane-associated cytokines. *Arthritis Rheum. 41:1748.*
43. Burger, D., and J. M. Dayer. 1999. Cytokines and direct cell contact in synovitis: relevance to therapeutic intervention. *Arthritis Res. 1:17.*

Lung (2004) 182:173–185
DOI: 10.1007/s00408-004-0309-1

Lung

Osteopontin is Strongly Expressed by Alveolar Macrophages in the Lungs of Acute Respiratory Distress Syndrome

Fumiyuki Takahashi,[1,2] Kazuhisa Takahashi,[1,2] Kazue Shimizu,[1,2] Ri Cui,[1,2] Norihiro Tada,[3] Hideki Takahashi,[1,2] Sanae Soma,[1,2] Masakata Yoshioka,[1,2] and Yoshinosuke Fukuchi[1,2]

[1]Department of Respiratory Medicine, Juntendo University School of Medicine, Hongo, Bunkyo-Ku, Tokyo, Japan; [2]Research Institute for Diseases of Old Ages, Tokyo, Japan; [3]Atopy Research Center, Juntendo University, School of Medicine, 2-1-1 Hongo, Bunkyo-Ku, Tokyo 113-8421, Japan

Abstract. Acute respiratory distress syndrome (ARDS) is characterized by an intense inflammatory response in the lung parenchyma. Recent studies suggest that excessive nitric oxide (NO) production mediated by inducible NO synthase (iNOS) in macrophages is partially involved in mediating acute lung injury in ARDS. On the other hand, osteopontin (OPN) is a cytokine which is capable of inhibiting NO production by suppressing iNOS mRNA expression in macrophages. In this study, we investigated the expression of OPN in the lungs of 10 patients with ARDS. In most patients, OPN is strongly expressed on alveolar macrophages. In addition, we produced a murine model for ARDS by intratracheal administration of lipopolysaccharide and investigated the expression of endogenous OPN and iNOS in the lungs of ARDS mice. Immunostaining demonstrated that *in vivo* OPN protein was coinduced with iNOS protein predominantly in the accumulating alveolar macrophages. OPN mRNA expression was also coinduced with iNOS mRNA, but was induced more slowly than iNOS mRNA in the lungs of ARDS mice. These results suggested that OPN, which may reduce NO production of macrophages by inhibiting iNOS expression, is significantly induced and expressed on alveolar macrophages in the lungs of ARDS. It is possible that OPN is partially involved in playing a protective role against excessive production of NO in ARDS.

Key words: Osteopontin—Macrophage—ARDS.

Correspondence to: Fumiyuki Takahashi; email: fumiyuki@med.juntendo.ac.jp

Introduction

Acute respiratory distress syndrome (ARDS) is characterized by an edematous reaction in the lung, leading to defective gas exchange, and carries a high mortality rate [1, 2]. ARDS frequently occurs following sepsis caused by gram-negative bacterial infection, aspiration of gastric contents, major trauma, or other clinical events [2]. Although many researchers have investigated the pathogenesis of ARDS, its cause remains largely unknown. Superoxide anion and proteolytic enzymes produced by activated neutrophils induce marked lung injury in ARDS [3–5]. Thus, the sequestration and subsequent activation of neutrophils in the lung are considered to be essential in the development of ARDS [1]. However, it has been demonstrated that neutrophil-depleted mice are still susceptible to lipopolysaccharide (LPS) in the development of ARDS [6].

Recent studies suggest that activated macrophages are also essential in the pathogenesis of ARDS. Stimulation of macrophages with LPS and various cytokines induces inducible nitric oxide synthase (iNOS) expression, resulting in elevated nitric oxide (NO) production [7]. The interaction of NO induced by iNOS with superoxide anion generated from macrophages or neutrophils forms a potent reactive oxidant, peroxynitrite, which induces severe tissue damage [8, 9]. It has therefore been suggested that increased output of NO production by alveolar macrophages stimulated with LPS is partially involved in mediating acute lung injury in ARDS. A number of studies support this hypothesis: Arkovits et al. [10] reported that selective iNOS inhibitors prevent pulmonary transvascular flux caused by LPS injection in a rat model Wu et al. [11] also demonstrated that the selective iNOS inhibitor aminoguanidine improves survival in an animal model for endotoxic shock induced by LPS. Similarly, lung damage after LPS injection is markedly reduced in iNOS-deficient mice compared with wild-type mice, as evaluated by the lung wet/dry ratio and lactate dehydrogenase content in BAL fluid [12]. These reports suggest that increased output of NO production mediated by iNOS from activated macrophages contributes to the development of acute lung injury/ARDS.

Osteopontin (OPN) is a secreted, arginine-glycine-asparatic acid (RGD)-containing phosphoglycoprotein with cell-adhesive and migratory properties [3, 14]. It has been demonstrated to be expressed in a variety of cells including cancer cells, osteoclasts, activated T cells, and activated macrophages [15–17]. Other than cell-adhesive and migratory functions, OPN has many other novel properties, suggesting that it may act as a cytokine and chemokine in various pathological conditions [18–20]. Recently, several investigators have demonstrated that OPN is capable of inhibiting NO production by suppressing iNOS expression in macrophages [21], renal epithelial cells [22], rat thoracic aorta [23], cardiac myocytes and microvascular endothelium [24]. It has been shown that endogenous OPN produced by activated macrophages inhibits cytotoxicity against tumor cells as a consequence of suppression of iNOS mRNA [21]. Scott et al. [23] reported that OPN suppresses iNOS activity in rat vascular tissues stimulated with LPS *in vitro*, suggesting that it may exert an anti-inflammatory effect during sepsis caused by gram-negative bacterial infection [23]. Singh et al. [24] demonstrated that glucocorticoids markedly

increase OPN mRNA and decrease iNOS mRNA in cardiac myocytes and microvascular endothelium (CMEC), suggesting that the suppression of iNOS by glucocorticoids in CMEC could be partially mediated by OPN [24].

These findings suggest that endogenous OPN may function as a counter-regulator of iNOS in a variety of pathological conditions. We previously reported that OPN and iNOS mRNA were coinduced in a murine macrophage cell line, RAW 264.7 cells, by treating the cells with LPS and IFN-γ [17]. In addition, OPN mRNA expression was markedly upregulated by NO generated from NO-releasing agents in RAW 264.7 cells [17]. We therefore hypothesized that OPN, which can reduce NO production of macrophages by inhibiting iNOS expression, is induced and expressed on alveolar macrophages in the lungs of ARDS, in which NO plays an important role.

In the present study, we examined OPN expression in the lungs of ARDS patients. In addition, we also produced a murine model for ARDS with LPS treatment and investigated the expression of OPN and iNOS in the lungs. We revealed that endogenous OPN is induced and strongly expressed by alveolar macrophages in the lungs of ARDS patients and murine experimental ARDS model.

Materials and Methods

Patients Characteristics and Tissue Preparation

Paraffin-embedded tissue sections were obtained from the postmortem lung samples of 10 patients (6 men, 4 women) with ARDS who were autopsied at Juntendo University Hospital. ARDS was confirmed according to the American European Consensus Conference definitions, which include acute onset of bilateral infiltrates on chest radiograph, an arterial pO_2-to-inspired O_2 ratio of ≤ 200, and no clinical evidence of elevated left arterial pressure [2]. The patients ranged in age from 36 to 85 years (mean ± S.D. 69.6 ± 15.0). Underlying diseases included sepsis, pneumonia, lung abscess, pulmonary embolism, acute pancreatitis, renal disease, cerebral hemorrhage, hematological disease, and malignant tumor. All patients had been treated with oxygen prior to death, and 4 had been ventilated mechanically. Normal lung tissue samples were obtained from 5 controls who had normal lung tissue surgically removed distal to the lung tumor. Tissue samples were formalin fixed, embedded in paraffin, and cut into 3 μm sections. Informed consent was obtained from either the patient or a responsible relative.

Animals

Specific pathogen-free male ICR mice aged 8 weeks were purchased from Charles River Laboratories, Japan (Tokyo, Japan). The mice were housed in filter-topped cages in an isolation room in the animal care facility with free access to rodent chow and water. All animal experiments were performed according to the Guidelines on Animal Experimentation as established by Juntendo University School of Medicine.

Intratracheal Inoculation of Echericha coli Lipopolysaccharide

Mice were anesthetized with pentobarbitral (50 mg/kg intraperitoneally). The trachea was exposed by midline incision into which a 24-gauge Saflow catheter® (Terumo, Tokyo, Japan) was introduced.

Then the mice were intratrachealy (i.t.) injected 10 μg of *E. coli* LPS (055: B5; Sigma, St. Louis, MI) or 0.05 ml phosphate-buffered saline (PBS). This was followed by 0.5 ml of air on days 0 and 4 on the basis of previous reports that single high-dose LPS injection failed to cause pulmonary edema in animal models, and that additional activation of macrophages, called "priming", was required to induce severe lung injury [7, 25]. The mice were sacrificed for RNA extraction from lungs 12 and 36 h after the second i.t. injection. Mortality rate for i.t. injection was less than 5%.

Bronchoalveolar Lavage (BAL)

Thirty-six hours after the second i.t. injection, bronchoalveolar lavage was performed. The animals were anesthetized before undergoing aortic transection. The sterile polypropylene catheter was secured in the trachea with suture material. The lungs were isolated and lavaged via the trachea with PBS. A total of 2 ml of lavage buffer was used per mouse in 0.5-ml increments. Total cell counts were assessed with a standard hemocytometer. Cellular populations were identified on air-dried cytocentrifuged smears (900 rpm × 2 min) after staining with Diff Quick stain (Wako, Tokyo, Japan). Similarly, treated slides were used for immunocytochemical analyses.

Immunostaining

The expression of OPN in the lungs of ARDS patients and the experimental murine model was assessed by immunohistochemical staining using mouse anti-human OPN monoclonal antibody (10A16; Immuno-Biological Laboratories Co.; Ltd.; Gunma, Japan) and polyclonal rabbit anti-human OPN antibody (IBL) which cross-reacts with mouse OPN, respectively. Immunohistochemical analyses were performed as previously described [16, 20]. Briefly, sections were autoclaved for 15 min at 120°C in 10 mM citrate buffer, pH 6.0 to retrieve the antigen. The sections were then incubated with mouse anti-human OPN antibody and rabbit anti-human OPN antibody diluted 1: 100 for 1 hr at room temperature (RT), respectively. Specific binding was detected through avidin-biotin peroxidase complex formation with a biotin-conjugated second antibody (Vectastain ABC Kit; Vector; Burlingame, CA) and diaminobendizine (Sigma; St. Louis, MI) as substrate. Staining was absent when isotype-matched immunoglobulin was used as the control.

The expression of iNOS in the lungs of ARDS mice was also assessed by immunohistochemical staining using polyclonal rabbit anti-mouse iNOS antibody (Affinity Bioreagents) according to the manufacturer's instructions. Alveolar macrophages were identified by immunoreactivity for anti-human CD68 antibody (Dako; Tokyo, Japan) and BM 8 antibody (BMA; Rheistrasse, Switzerland) which reacts specifically to human and murine macrophages, respectively. Immunohistochemical staining was conducted according to the manufacturer's instructions, whereby, BAL cells were fixed with cold acetone and subjected to the same method as that for immunohistochemistry. Each specimen was examined independently by three observers. In order to prevent observer's bias, samples were coded and examined in a blind manner.

Northern Blot

iNOS cDNA probe was purchased from Cayman Chemical (Ann Arbor, MI). OPN cDNA was amplified from RAW 264.7 cells. Sense primer (5′-GCCTGGATCCTCCCGGTGAAAGTGACT-GAT-3′) contains the *Bam*HI restriction site and the cDNA sequence coding the first seven amino acids of mature OPN. Anti-sense primer AS1 (5′-GTTAGAATTCCTGCTTAATCCTCACTAACA-3′) contains the *Eco*RI restriction site and the cDNA sequence of the six amino acids starting from 19 amino acids C-terminal from the stop codon. Nuclear sequences of the cDNA were verified with a DNA sequencer (Perkin Elmer; Foster City, CA). The PCR product was digested with *Bam*HI and

*Eco*RI, and subcloned into the *Bam*HI and *Eco*RI sites of the pGEX-5X1 vector (Amersham Pharmacia Biotech; Buckinghamshire, England). The template was used as a probe for Northern blots. Total RNAs were extracted from lungs and cells by the guanidium thiocyanate-phenol-chloroform extraction procedure (Tel-test; Friendswood, TX). Total RNAs were electrophoresed in 1% formaldehyde agarose gel and transferred onto a nylon membrane (Amersham Pharmacia Biotech). cDNA probes were labeled with [^{32}P]dCTP (Amersham Pharmacia Biotech) by the random prime method (Takara; Tokyo, Japan).

Prehybridization and hybridization were carried out at 42°C overnight. Filters were washed in 2× SSC, 0.1% SDS twice and in 0.1 × SSC, 0.1% SDS 4 times at 55°C and exposed to the film (Fuji Film; Tokyo, Japan). Filters were also hybridized with a human 28 S ribosomal RNA cDNA probe as a control for loading. Autoradiography bands were quantitated by image analyzer (Fuji Film; Tokyo, Japan).

Measurement of NO Production

NOx, nitrite and nitrate, were determined with an NOx assay kit (Boehringer Mannheim; Mannheim, Germany) according to the manufacturer's instruction [7]. Briefly, 50 µl of BAL fluid, sera, and culture supernatants were reacted with 1 U/ml nitrate reductase and 1 mg/ml NADPH, followed by incubation with an equal volume of Griess reagent (1% sulfanilamide, 0.1% N-1-naphthylethylenediamine dihydrochloride, and 2.5% phosphoric acid) at room temperature for 5 min. Absorbance at 560 nm was determined with a microplate reader (Bio-Rad; Hercules, CA). NOx concentrations were calculated from a standard sodium nitrite curve. All samples were analyzed in triplicate.

Myeloperoxidase Assay

Myeloperoxidase (MPO) was analyzed as described previously [26, 27, 28]. Briefly, 0.12 ml BAL fluid was mixed with 0.88 ml substrate solution (0.1 M citric acid-sodium citrate buffer, pH 5.0, 0.1% o-tolidine in ethanol, 1.5 mM H_2O_2), and absorbance at 440 nm was measured.

Statistics

Statistical analyses were performed by analysis of variance (ANOVA). All data are presented as mean ± S.D. Differences between means were considered statistically significant at $p < 0.05$.

Results

OPN Expression in Lungs of Patients with ARDS

OPN expression was investigated in lung tissues from 10 patients with ARDS. Pathological findings of these patients revealed diffuse alveolar damage, with neutrophils, macrophages, hyaline membranes, protein-rich edema fluid in the alveolar spaces, and disruption of the alveolar epithelium (data not shown). These findings suggested ARDS. Tissue sections were stained with anti-human OPN mAb (clone 10A16) or isotype-matched IgG. As shown in Figure 1A, OPN was strongly expressed by accumulating macrophages in alveolar spaces. Interestingly,

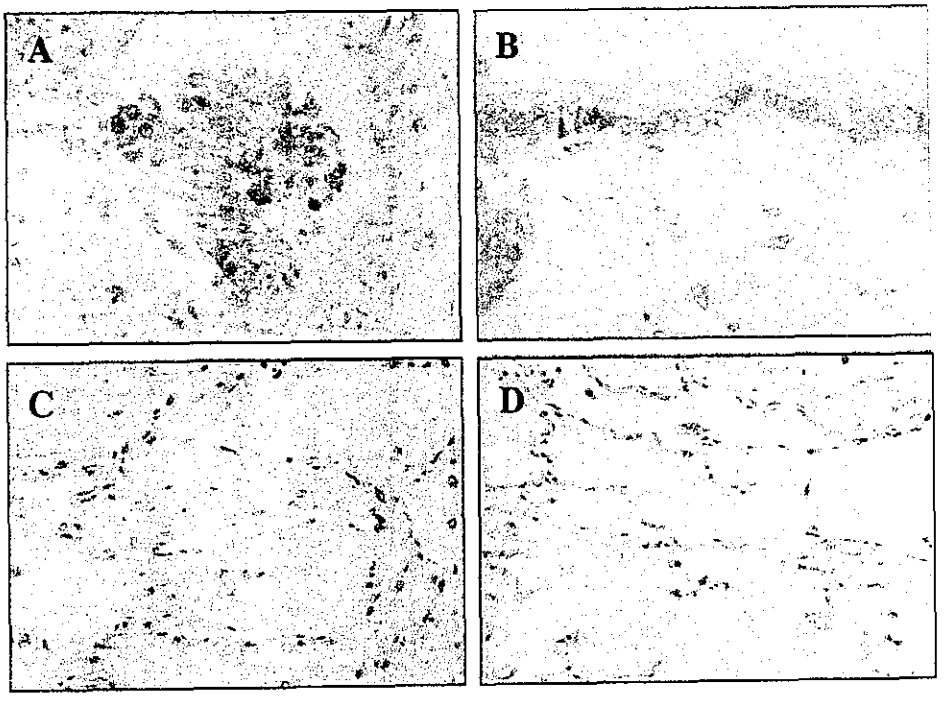

Fig. 1. Immunohistochemical staining of OPN in the lungs of ARDS patients and controls. The lung tissues obtained from ARDS patients (**A**, **B**, **C**) and controls (**D**) were stained with antibody against OPN. (**A**) OPN was strongly expressed on macrophages in alveolar spaces in the lungs of ARDS patients. Alveolar epithelial cells were weakly stained for OPN. No staining was observed in (**B**) bronchial epithelial cells, (**C**) vascular endothelial and smooth muscle cells in the lungs of ARDS patients, and (**D**) alveolar macrophages in the lungs of controls. Hematoxylin was used as the counter stain (original magnification: ×100).

OPN-expressing macrophages were aggregated. Interstitial macrophages were weakly stained for OPN.

In contrast, no significant staining was observed on lymphocytes and neutrophils. To verify that OPN-producing cells were indeed macrophages, immunostaining using an antibody against human macrophage antigen CD68 was conducted. OPN-expressing cells were also stained with a mAb specific for CD68, indicating that OPN was expressed predominantly on alveolar macrophages (data not shown). Alveolar epithelial cells were weakly stained for OPN (Fig. 1A). OPN expression on bronchial epithelium, vascular endothelial cells, and smooth muscle cells were not significant (Fig. 1B, C). No staining of these specimens was observed with the isotype control Ab. Normal control lungs did not demonstrate any significant staining for OPN (Fig. 1D). Cellular expression and localization of OPN are summarized in Table 1. These results indicated that OPN was induced and expressed predominantly on alveolar macrophages in the lungs of patients with ARDS.

Table 1. Cellular expression and localization of OPN in the lungs of ARDS patients and normal controls

	ARDS patients (n = 10)	Normal controls (n = 5)
Alveolar macrophages	+ + +	–
Interstitial macrophages	+	–
Lymphocytes	–	–
Neutrophils	–	–
Bronchial epithelial cells	–	–
Alveolar epithelial cells	+	–
Vascular endothelial cells	–	–
Vascular smooth muscle cells	–	–

Staining intensities were scored according to the following scale: –, no staining; +, weak staining; + +, positive staining, + + +, strong staining

Experimental ARDS in Mice

We produced a murine model for ARDS by sequential exposure to LPS. Confirmation of ARDS was conducted with both histological and biochemical analyses. Histological examination of the lungs at 36 h after LPS treatment revealed alveolar wall thickening, edema, parenchymal damage, and accumulation of neutrophils and macrophages in the interstitium, all of which are consistent with ARDS (data not shown). In contrast, PBS-treated mice demonstrated normal lung findings. Wet lung weights were significantly higher in LPS-treated than in PBS-treated mice (Table 2). We next performed bronchoalveolar lavage (BAL). LPS treatment resulted in an increased number of neutrophils and macrophages compared to PBS treatment (Table 2). Protein levels and MPO activity in BAL fluid of LPS-treated mice were also increased (Table 2). We also measured NO_2^-/NO_3^- (NOx) levels in BAL fluid and sera in these mice. Levels of NOx in both BALF and sera of LPS-treated mice were significantly higher than those of the control mice.

Immunostaining of OPN and iNOS Proteins in ARDS Mice Lungs and Bronchoalveolar Lavage Cells

Immunohistochemical analyses were carried out on the lungs obtained at 36 h after the second i.t. injection. OPN and iNOS proteins were absent in the lungs of PBS-treated mice (data not shown). In contrast, alveolar macrophages in the lungs of LPS-treated mice were positive for OPN and iNOS immunoreactivity (data not shown). To further identify cells positive for OPN and iNOS proteins in the lungs of LPS- or PBS-treated mice, immunocytochemical analyses were also performed on BAL cells (Fig. 2). We first ascertained that aggregated cells were identified as alveolar macrophages by positive immunoreactivity to BM 8 antibody (data not shown). As expected, both iNOS and OPN proteins were strongly positive predominantly in the alveolar macrophages (Fig. 2A, B). Neither iNOS nor OPN

Table 2. Comparison of wet lung weight, number of neutrophils and macrophages, and biochemical parameters of acute lung injury between in LPS- and PBS-treated mice

	Wet lung weight[a] (mg)	Neutrophils in BAL[b] ($\times 10^3$/ml)	Macrophages in BAL[b] ($\times 10^4$/ml)	Protein in BAL fluid[c] (mg/ml)	MPO activity in BALF[d] (ΔOD440/min)	NOx in BALF[e] (μM)	NOx in serum[e] (μM)
LPS	162 ± 28**	1250 ± 54***	30 ± 16**	1.46 ± 0.6**	0.017 ± 0.01**	4.8 ± 1.5**	63 ± 57*
PBS	65 ± 12	4.8 ± 8.2	6.5 ± 0.9	0.065 ± 0.01	0.0005 ± 0.0005	2.2 ± 0.5	33 ± 32

[a] $n = 4$ for LPS i.t., $n = 4$ for PBS i.t.
[b] $n = 6$ for LPS i.t., $n = 5$ for PBS i.t.
[c] $n = 6$ for LPS i.t., $n = 8$ for PBS i.t.
[d] $n = 6$ for LPS i.t., $n = 7$ for PBS i.t.
[e] $n = 6$ for LPS i.t., $n = 7$ for PBS i.t.*$p < 0.05$ vs. PBS i.t. **$p < 0.01$ vs. PBS i.t. ***$p < 0.001$ vs. PBS i.t.

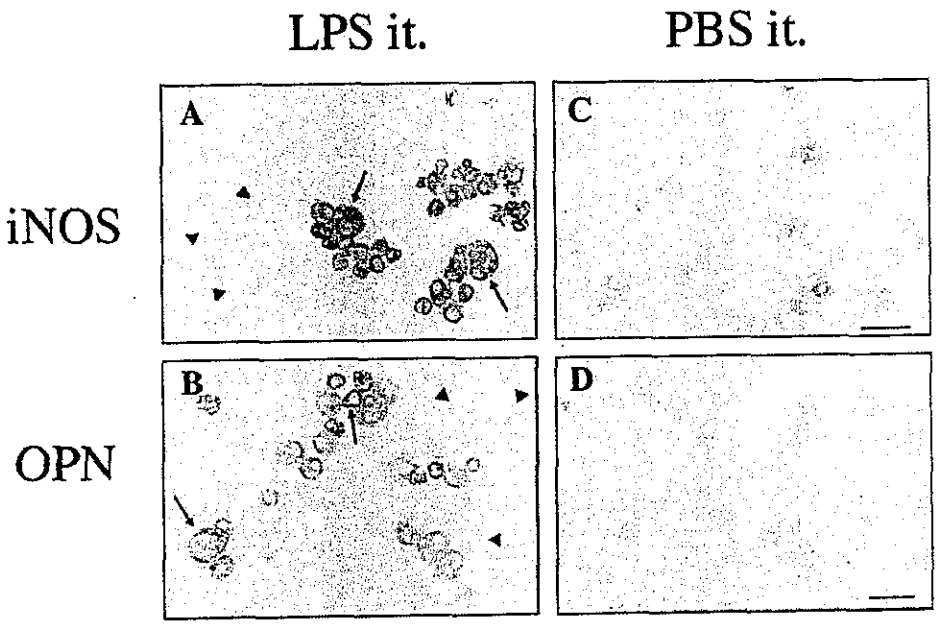

Fig. 2. Immunocytochemical staining of BAL cells from LPS- and PBS-treated mice for iNOS (A, C) and OPN (B, D) protein. BAL cells recovered from mice at 36 h after the second i.t. injection with LPS or PBS which were stained with a polyclonal antibody against iNOS (A: LPS, C: PBS) or OPN (B: LPS, D: PBS). Arrows indicate macrophages showing positive staining for iNOS and positive staining for OPN. Arrowheads indicate neutrophils showing negative staining for iNOS and for OPN. Bar indicates 10 μm in Figures 2C and 2D.

were prominent in neutrophils (Fig. 2A, B) or all BAL cells obtained from PBS-treated mice (Fig. 2C, D) These data indicate that OPN and iNOS proteins were coinduced predominantly in alveolar macrophages in the lungs of ARDS mice.

Expression of OPN and iNOS mRNA in Lungs of ARDS Mice

We also investigated the expression of OPN and iNOS mRNA in the whole lungs after LPS treatment *in vivo* (Fig. 3A, B). iNOS mRNA reached its maximum at 12 h after treatment and then decreased rapidly at 36 h. In contrast, OPN mRNA began to increase at 12 h with a lag time and was prominent at 36 h. Thus, iNOS and OPN mRNAs were coinduced by LPS in the lungs, but OPN mRNA was induced more slowly than iNOS mRNA. In contrast, neither mRNAs were induced in the lungs after PBS treatment (data not shown).

Discussion

In the current study, we revealed that OPN is strongly expressed by alveolar macrophages in the lungs of ARDS patients. In addition, we produced a murine

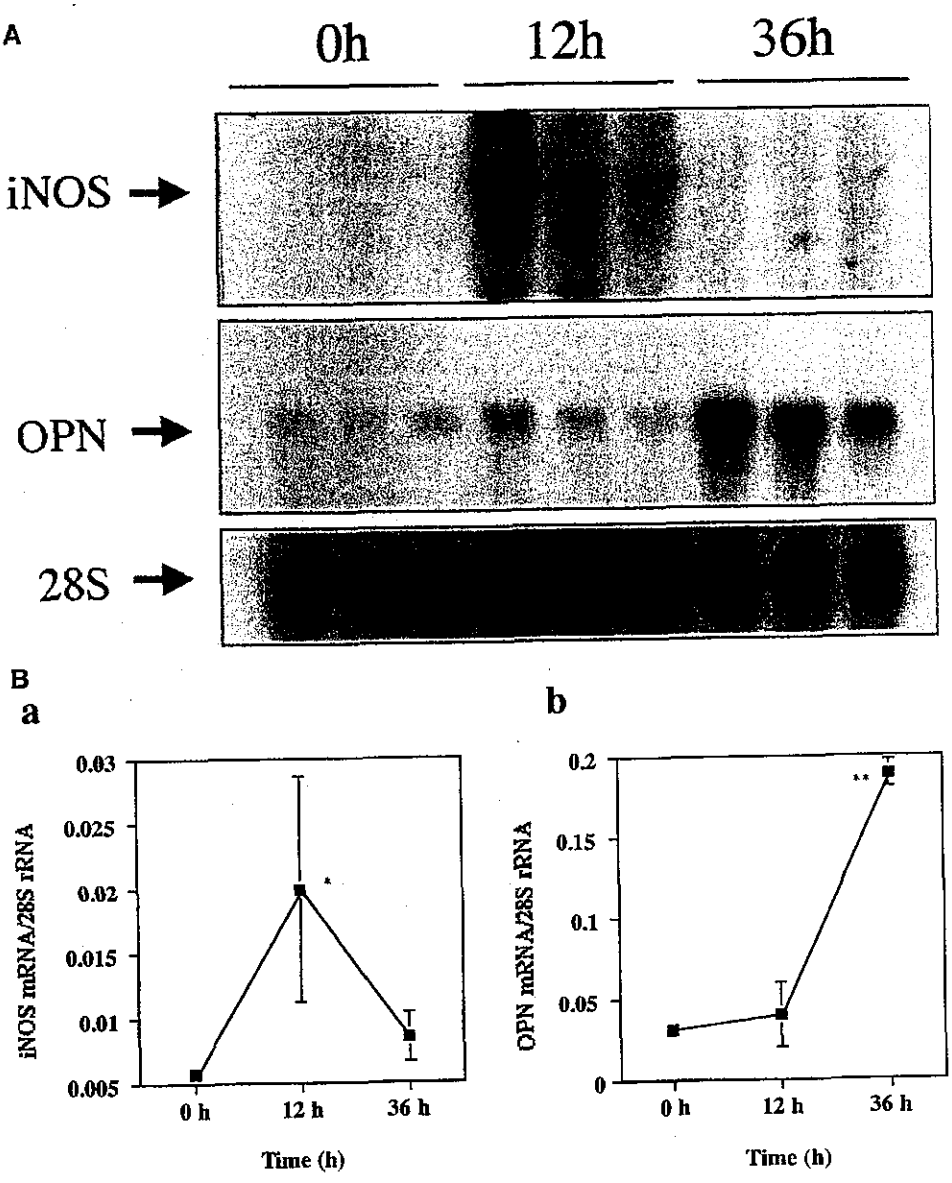

Fig. 3. Induction of iNOS and OPN mRNA in the lungs of LPS-treated mice with Northern blot. (A) Total RNAs were isolated from lungs of 3 mice at the indicated time period (h) after treatment with LPS (10 μg/50 μl) or PBS (50 μl). RNAs (10 μg) were subjected to blot analysis. Upper panels indicate the expression of iNOS or OPN mRNA. Lower panel shows 28S rRNA as the control. (B) The signals were quantified using a computerized image analyzer. Calculated ratios iNOS/28S signal (a) and OPN/28S signal (b) are shown in Figure 3B. Data are presented as the mean ± SD of three independent experiments. $^{*}p < 0.05$ vs. time 0, $^{**}p < 0.001$ vs. time 0.

model for ARDS with LPS treatment and investigated the expression of OPN and iNOS in the lungs. OPN protein was significantly induced by alveolar macrophages and OPN mRNA was induced more slowly than iNOS mRNA. These results, together with previous findings, suggest that OPN, which can reduce NO production of macrophages by inhibiting iNOS expression, is significantly induced and strongly expressed on alveolar macrophages in the lungs of ARDS. Although we were unable to demonstrate direct evidence that OPN is implicated in the pathogenesis of ARDS, it is possible that it has beneficial effects in protecting lung tissues from damage by reactive nitrogen intermediates by inhibiting iNOS expression in macrophage.

What actually induces and upregulates OPN expression in the lungs of ARDS is unclear. Previous reports have indicated that tumor necrosis factor-α (TNF-α) plays a key role in the pathogenesis of ARDS [1]. The expression of OPN mRNA was revealed to be increased in the macrophage cell line in the presence of TNF-α, as well as in alveolar macrophages in transgenic mice that were engineered to express TNF-α in type II pneumocytes [29]. Other than TNF-α, various mediators, including IL-1β, PDGF, and TGF-β, have also been demonstrated to upregulate OPN transcription and stimulate OPN expression [30]. It has been demonstrated that iNOS is strongly expressed on alveolar macrophages of human lungs predominantly during the early stage of ARDS following sepsis [31]. In addition, increased levels of NO production were demonstrated in the lungs of ARDS patients [32]. We have previously reported that increased amounts of NO generated by NO-releasing agents directly upregulates OPN expression in the murine macrophage cell line [17]. Therefore, induction of OPN appears to be mediated by NO and/or various inflammatory mediators induced in the lungs of ARDS.

Kinetic studies in a murine experimental model revealed that OPN mRNA is induced much more slowly and with a time lag in the lungs of LPS-treated mice, whereas iNOS mRNA is induced more rapidly. Immunohistochemical studies suggested that OPN mRNA were mainly derived from macrophages. We previously reported that iNOS and OPN are coinduced in the murine macrophage cell line stimulated with LPS and IFN-γ, and induction of OPN mRNA was also slower than that of iNOS mRNA *in vitro* [17]. Thus, the profile of kinetics for iNOS and OPN mRNA induction *in vivo* resembled that of an *in vitro* murine macrophage cell line on treatment of cells with LPS and IFN-γ. We also previously demonstrated that OPN mRNA induction was markedly suppressed by inhibiting iNOS mRNA by addition of the specific iNOS inhibitor S-2-aminoethyl isothiourea dihydrobromide. Moreover, OPN mRNA expression was significantly upregulated by NO generated by NO-releasing agent spermine NONOate. Guo et al. also demonstrated that OPN gene transcription and promotor activity is upregulated by NO in endotoxin- and cytokine- stimulated macrophages [33]. These findings suggested that NO generated by iNOS upregulates OPN expression in macrophages stimulated with LPS. Together with these previous findings, it is possible that delayed induction of OPN is caused by excessive production of NO by macrophages in ARDS.

Conclusively, our study revealed that OPN is significantly induced and strongly expressed on alveolar macrophages in the lungs of ARDS patients and a

murine experimental model. Our data suggest that induced OPN may have beneficial effects, protecting tissue from damage by toxic reactive nitrogen intermediates, by inhibiting iNOS expression in macrophages. However, further studies are necessary.

Acknowledgments. We thank Dr. Y. Ishii for her excellent advise. This work was supported in part by Grant-in-Aid for Scientific Research 13670616 (K.T.) and 14770279 (F.T.) from the Ministry of Education, Culture, Sports, Science, and Technology of Japan.

References

1. Ware LB, Matthay MA (2000) The acute respiratory distress syndrome. N Engl J Med 342:1334–1349
2. Bernard GR, Artigas A, Brigham KL, et al. (1994) The American-European Consensus Conference on ARDS. Definitions, mechanisms, relevant outcomes, and clinical trial coordination. Am J Respir Crit Care Med 149:818–824
3. Hogg JC (1987) Neutrophil kinetics and lung injury. Physiol Rev 67:1249–1295
4. Lee CT, Fein AM, Lippmann M, Holtzman H, Kimbel P, Weinbaum G (1981) Elastolytic activity in pulmonary lavage fluid from patients with adult respiratory-distress syndrome. N Engl J Med 304:192–196
5. Thommasen HV, Russell JA, Boyko WJ, Hogg JC (1984) Transient leucopenia associated with adult respiratory distress syndrome. Lancet 1:809–812
6. Tasaka S, Ishizaka A, Urano T, et al. (1995) BCG priming enhances endotoxin-induced acute lung injury independent of neutrophils. Am J Respir Crit Care Med 152:1041–1049
7. Shellito JE, Kolls JK, Summer WR (1995) Regulation of nitric oxide release by macrophages after intratracheal lipopolysaccharide. Am J Respir Cell Mol Biol 13:45–53
8. Wizemann TM, Gardner CR, Laskin JD, et al. (1994) Production of nitric oxide and peroxynitrite in the lung during acute endotoxemia. J Leukoc Biol 56:759–768
9. Beckman JS, Beckman TW, Chen J, Marshall PA, Freeman BA (1990) Apparent hydroxyl radical production by peroxynitrite: implications for endothelial injury from nitric oxide and superoxide. Proc Natl Acad Sci USA 87:1620–1624
10. Arkovitz MS, Wispe JR, Garcia VF, Szabo C (1996) Selective inhibition of the inducible isoform of nitric oxide synthase prevents pulmonary transvascular flux during acute endotoxemia. J Pediatr Surg 31:1009–1015
11. Wu CC, Chen SJ, Szabo C, Thiemermann C, Vane JR (1995) Aminoguanidine attenuates the delayed circulatory failure and improves survival in rodent models of endotoxic shock. Br J Pharmacol 114:1666–1672
12. Kristof AS, Goldberg P, Laubach V, Hussain SN (1998) Role of inducible nitric oxide synthase in endotoxin-induced acute lung injury. Am J Respir Crit Care Med 158:1883–1889
13. Denhardt DT, Guo X (1993) Osteopontin: a protein with diverse functions. Faseb J 7:1475–1482
14. Takahashi K, Takahashi F, Tanabe KK, Takahashi H, Fukuchi Y (1998) The carboxyl-terminal fragment of osteopontin suppresses arginine-glycine-asparatic acid-dependent cell adhesion. Biochem Mol Biol Int 46:1081–1092
15. Denhardt DT, Noda M, O'Regan AW, Pavlin D, Berman JS (2001) Osteopontin as a means to cope with environmental insults: regulation of inflammation, tissue remodeling, and cell survival. J Clin Invest 107:1055–1061
16. Zhang J, Takahashi K, Takahashi F, et al. (2001) Differential osteopontin expression in lung cancer. Cancer Lett 171:215–222
17. Takahashi F, Takahashi K, Maeda K, Tominaga S, Fukuchi Y (2000) Osteopontin is induced by nitric oxide in RAW 264.7 cells. IUBMB Life 49:217–221

18. O'Regan AW, Chupp GL, Lowry JA, Goetschkes M, Mulligan N, Berman JS (1999) Osteopontin is associated with T cells in sarcoid granulomas and has T cell adhesive and cytokine-like properties *in vitro*. J Immunol 162:1024–1031
19. Takahashi F, Akutagawa S, Fukumoto H, et al. (2002) Osteopontin induces angiogenesis of murine neuroblastoma cells in mice. Int J Cancer 98:707–712
20. Takahashi F, Takahashi K, Okazaki T, et al. (2001) Role of osteopontin in the pathogenesis of bleomycin-induced pulmonary fibrosis. Am J Respir Cell Mol Biol 24:264–271
21. Rollo EE, Laskin DL, Denhardt DT (1996) Osteopontin inhibits nitric oxide production and cytotoxicity by activated RAW264.7 macrophages. J Leukoc Biol 60:397–404
22. Hwang SM, Lopez CA, Heck DE, et al. (1994) Osteopontin inhibits induction of nitric oxide synthase gene expression by inflammatory mediators in mouse kidney epithelial cells. J Biol Chem 269:711–715
23. Scott JA, Weir ML, Wilson SM, Xuan JW, Chambers AF, McCormack DG (1998) Osteopontin inhibits inducible nitric oxide synthase activity in rat vascular tissue. Am J Physiol 275:H2258–H2265
24. Singh K, Balligand J, Fisher T, Smith TW, Kelly RA (1995) Glucocorticoids increase osteopontin expression in cardiac myocytes and microvascular endothelial cells. J Biol Chem 270:28471–28478
25. Wollert PS, Menconi MJ, Wang H, et al. (1994) Prior exposure to endotoxin exacerbates lipopolysaccharide-induced hypoxemia and alveolitis in anesthetized swine. Shock 2:362–369
26. Szarka RJ, Wang N, Gordon L, Nation PN, Smith RH (1997) A murine model of pulmonary damage induced by lipopolysaccharide via intranasal instillation. J Immunol Methods 202:49–57
27. Baggiolini M, Hirsch JG, De Duve C (1969) Resolution of granules from rabbit heterophil leukocytes into distinct populations by zonal sedimentation. J Cell Biol 40:529–541
28. Avila JL, Convit J (1973) Studies on human polymorphonuclear leukocyte enzymes. I. Assay of acid hydrolases and other enzymes. Biochim Biophys Acta 293:397–408
29. Miyazaki Y, Tashiro T, Higuchi Y, et al. (1995) Expression of osteopontin in a macrophage cell line and in transgenic mice with pulmonary fibrosis resulting from the lung expression of a tumor necrosis factor-alpha transgene. Ann N Y Acad Sci 760:334–341
30. Rodan GA (1995) Osteopontin overview. Ann N Y Acad Sci 760:761–765
31. Kobayashi A, Hashimoto S, Kooguchi K, et al. (1998) Expression of inducible nitric oxide synthase and inflammatory cytokines in alveolar macrophages of ARDS following sepsis. Chest 113:1632–1639
32. Sittipunt C, Steinberg KP, Ruzinski JT, et al. (2001) Nitric oxide and nitrotyrosine in the lungs of patients with acute respiratory distress syndrome. Am J Respir Crit Care Med *163:503–510*
33. Guo H, Cai CQ, Schroeder RA, Kuo PC (2001) Osteopontin is a negative feedback regulator of nitric oxide synthesis in murine macrophages. J Immunol 166:1079–1086

Accepted for publication: April 12, 2004

Dissection of the role of MHC class II A and E genes in autoimmune susceptibility in murine lupus models with intragenic recombination

Danqing Zhang*, Keishi Fujio†, Yi Jiang‡, Jingyuan Zhao*, Norihiro Tada§, Katsuko Sudo¶, Hiromichi Tsurui*, Kazuhiro Nakamura*, Kazuhiko Yamamoto†, Hiroyuki Nishimura‖, Toshikazu Shirai*, and Sachiko Hirose*,**

*Second Department of Pathology and §Atopy Research Center, Juntendo University School of Medicine, Tokyo 113-8421, Japan; †Department of Allergy and Rheumatology, Graduate School of Medicine, University of Tokyo, Tokyo 113-0033, Japan; ‡Central Laboratory of First Clinical College, China Medical University, ShenyCang 110001, China; ¶Animal Research Center, Tokyo Medical University, Tokyo 160-8402, Japan; and ‖Toin Human Science and Technology Center, Department of Biomedical Engineering, Toin University of Yokohama, Yokohama 225-8502, Japan

Communicated by N. Avrion Mitchison, University College London, London, United Kingdom, August 8, 2004 (received for review July 7, 2004)

Systemic lupus erythematosus (SLE) is a multigenic autoimmune disease, and the major histocompatibility complex (MHC) class II polymorphism serves as a key genetic element. In SLE-prone (NZB × NZW)F_1 mice, the MHC H-$2^{d/z}$ heterozygosity (H-2^d of NZB and H-2^z of NZW) has a strong impact on disease; thus, congenic H-$2^{d/d}$ homozygous F_1 mice do not develop severe disease. In this study, we used *Ea*-deficient intra-H-2 recombination to establish $A^{d/d}$-congenic (NZB × NZW)F_1 mice, with or without E molecule expression, and dissected the role of class II A and E molecules. Here we found that $A^{d/d}$ homozygous F_1 mice lacking E molecules developed severe SLE similar to that seen in wild-type F1 mice, including lupus nephritis, autoantibody production, and spontaneously occurring T cell activation. Additional evidence revealed that E molecules prevent the disease in a dose-dependent manner; however, the effect is greatly influenced by the haplotype of A molecules, because wild-type H-$2^{d/z}$ F_1 mice develop SLE, despite E molecule expression. Studies on the potential of dendritic cells to present a self-antigen chromatin indicated that dendritic cells from wild-type F_1 mice induced a greater response of chromatin-specific T cells than did those from $A^{d/d}$ F_1 mice, irrespective of the presence or absence of E molecules, suggesting that the self-antigen presentation is mediated by A, but not by E, molecules. Our mouse models are useful for analyzing the molecular mechanisms by which MHC class II regions regulate the process of autoimmune responses.

Systemic lupus erythematosus (SLE) is a systemic autoimmune disease characterized by the appearance of autoantibodies to several nuclear components. The deposition of formed immune complexes mediates the disease in a wide variety of tissues and organs, including the kidney and the vascular system. There is evidence that the development of SLE is under the control of multiple susceptibility genes (1). Among these, genes in the major histocompatibility complex (MHC) have been implicated as a key genetic element. Because SLE is an autoantibody-mediated disease, MHC class II polymorphisms are probably involved in the pathogenesis. However, because of the complex multifactorial inheritance and heterogeneity of SLE, and because of the linkage disequilibrium that exists among the class I, II, and III genes within the MHC complex, the absolute contribution of individual MHC class II loci has been difficult to dissect. Thus, our knowledge of the molecular mechanism of MHC class II contribution to SLE remains incomplete.

Substantial progress in research in this area has been achieved through studies using SLE-prone mice with genetic recombination and manipulation of MHC (H-2) genes. In (NZB × NZW)F_1 mice that spontaneously develop disease closely resembling human SLE, the disease is strongly associated with H-2 haplotypes from both parents (H-2^d from NZB and H-2^z from NZW) (2–6). Genetic dissection by producing H-2-congenic mice revealed that an early onset of severe SLE occurs in only heterozygous H-$2^{d/z}$ mice and not in homozygous H-$2^{d/d}$ and H-$2^{z/z}$ mice (2, 3, 5). Although both A and E class II molecules may be involved, evidence has suggested that mixed haplotype class II $A\alpha^d\beta^z$ molecules are responsible for the pathogenesis by promoting the production of pathogenic high-affinity IgG autoantibodies to nuclear components (7, 8).

In contrast to class II A molecules, E molecules are suggested to be a suppressive genetic element for SLE. This notion was based mainly on the results obtained by using a transgene technique. A BXSB strain of mouse, another spontaneous SLE model, carries H-2^b haplotype and expresses A^b, but not E, molecules, because of a defect in the *Ea* gene (9). The development of BXSB disease is closely associated with the H-2^b haplotype (10) and is almost completely prevented by a transgene encoding $E\alpha^d$ chains (11). Similar findings were noted in the nonobese diabetic (NOD) mouse, a model of spontaneous autoimmune diabetes. NOD mice express class II A^{g7}, but not E, molecules, because of a defect in the *Ea* gene (12). Evidence indicated that whereas the class II A^{g7} gene is critical for the disease susceptibility (13), the transgenic introduction of $E\alpha^d$ or $E\alpha^k$ does prevent the disease (14–16). Thus, A and E molecules seem to provide the susceptible and protective genetic elements for autoimmune diseases, respectively, at least in these mouse models.

Nevertheless, the conclusion awaits further studies, because the transgene possibly induces unexpected improper effects on immune cells. For example, unpaired or mispaired transgene-derived class II molecules can be toxic to B cell maturation (17). Furthermore, there are reports suggesting that excessively generated transgenic $E\alpha^d$ molecules bind to A molecules, thereby decreasing the availability of A molecules for antigen presentation (18), and that overexpression of E molecules suppresses expression levels of endogenously encoded A molecules (19). In the (NZB × NZW)F_1 model, severe SLE occurs despite the presence of intact E molecules. To examine the role of A and E molecules in (NZB × NZW)F_1 lupus, we generated several kinds of congenic (NZB × NZW)F_1 mice with intra-MHC recombination at the *E* subregion, taking advantage of natural recombinants, including those we found among ≈3,000 meiosis in crosses of NZB strains.

Materials and Methods

Mice. NZB (H-2^d) and NZW (H-2^z) mice were purchased from the Shizuoka Laboratory Animal Center (Shizuoka, Japan) and were maintained in our animal facility. The H-2-congenic

Abbreviations: DC, dendritic cell; NOD, nonobese diabetic; SLE, systemic lupus erythematosus; TCR, T cell receptor.

**To whom correspondence should be addressed at: Second Department of Pathology, Juntendo University School of Medicine, 2-1-1, Hongo, Bunkyo-ku, Tokyo 113-8421, Japan. E-mail: sacchi@med.juntendo.ac.jp.

www.pnas.org/cgi/doi/10.1073/pnas.0405807101

Table 1. H-2 haplotypes of established MHC-congenic and intra-MHC recombinant-congenic New Zealand strains of mice

Strains	H-2 haplotype	*K*	*Ab*	*Aa*	*Eb*		*Ea*		*Tnfa*	*D*
NZB	d	d	d	d	d		d		d	d
NZB.GD	g2	d	d	d	d	//	b		b	b
NZW.GD	g2	d	d	d	d	//	b		b	b
NZB.GDr	g2r	d	d	d	d		d	//	b	b
NZW.H-2^d	d	d	d	d	d		d		d	d
(NZB × NZW.H-2^d)F_1	d/d	d	d	d	d		d		d	d
(NZB × NZW.GD)F_1	d/g2	d	d	d	d		d/b		d/b	d/b
(NZB.GDr × NZW.GD)F_1	g2r/g2	d	d	d	d		d/b		b	b
(NZB.GD × NZW.GD)F_1	g2/g2	d	d	d	d	//	b		b	b

//, Intra-H-2 recombination site between d and b haplotype.

NZW.H-2^d (2, 3, 5) strain was established by selective backcrossing of (NZB × NZW)F_1 to NZW for 15 generations. NZB.GD (H-2^{g2}) (20) and NZW.GD strains were established by selective backcrossing of (B10.GD × NZB)F_1 and (B10.GD × NZW)F_1 with NZB and with NZW mice, respectively, for 15 generations. The NZB strain with an intragenic recombination between *Ea* of NZB and *Tnfa* of NZB.GD was obtained in crosses of NZB and NZB.GD strains and was tentatively designated NZB.GDr. Alleles at the H-2 loci in established H-2-congenic and recombinant H-2-congenic New Zealand mice are shown in Table 1. These mice were crossed to produce (NZB × NZW)F_1 hybrids with the same d haplotype of the upstream region of the *Eb* gene but with different haplotypes of downstream regions of the *Ea* gene (Table 1), and the disease severity was compared among these female F_1 mice.

Typing of H-2 Haplotype. Peripheral blood was obtained from the periorbital sinus, followed by lysis of red blood cells with ammonium chloride. Aliquots of 5×10^5 to 10×10^5 cells were incubated with anti-A^d (*K24–199*) (21); anti-E (ISCR, which reacts with a common determinant of the E molecule) (a kind gift from Dr. N. Shinohara, Kitasato University, Kanagawa, Japan); anti-D^d (T19–191); and anti-D^b (H141–30) mAbs, followed by FITC-labeled anti-mouse polyclonal IgG antibodies (ICN). Incubations were run for 30 min at 4°C, and the stained cells were analyzed by using FACSTAR and CELLQUEST software (Becton Dickinson).

Microsatellite DNA Polymorphism in the *Tnfa* Promoter. *Tnfa* promoter was shown to have microsatellite polymorphism, and different tumor necrosis factor alleles have different lengths of microsatellites (22, 23). To determine the tumor necrosis factor alleles of each mouse strain, PCRs were performed with genomic DNAs, using 5′ primer (5′-GGACAGAGAAGAAATGGGTTTC-3′) and 3′ primer (5′-TCGAATCTGGGGCCAATCAGGAGGG-3′) (22), and differences in lengths of PCR products were determined by using electrophoresis of PCR products on 7% denaturing polyacrylamide gels, as described in ref. 24.

Measurement of Proteinuria. The onset of renal disease was monitored by biweekly testing for proteinuria, as described in ref. 25. Mice with a proteinuria of 111 mg/ml or more in repeated tests were regarded as being positive.

Measurements of Anti-DNA and Anti-Chromatin Antibodies. Serum levels of IgG autoantibodies to DNA and chromatin were determined by ELISA, using peroxidase-conjugated polyclonal anti-mouse IgG antibodies (ICN). The DNA- and chromatin-binding activities were expressed in units, referring to a standard curve obtained by serial dilutions of a standard serum pool from 7- to 9-month-old (NZB × NZW)F_1 mice, containing 1,000 units/ml (5). DNA was obtained from calf thymus (Sigma). Chromatin was prepared as described in ref. 26. Briefly, nucleosomes were isolated by solubilizing chromatin from purified chicken erythrocyte nuclei with micrococcal nuclease. The solubilized chromatin was fractionated into sucrose gradients that were analyzed for monomers by using electrophoresis, and the appropriate fractions were dialyzed and pooled.

Analysis of T Cell Activation and T Cell Receptor (TCR) V_β Repertoires. To examine the activation states of $CD4^+$ T cells, aliquots of 10^6 spleen cells were double-stained with FITC-conjugated anti-CD4 mAb and phycoerythrin-conjugated anti-CD69 mAb. To analyze TCR V_β repertoires, spleen cells were stained with biotin-labeled mAbs to each TCR V_β repertoire (Pharmingen), followed by incubation with avidin-phycoerythrin and FITC-conjugated anti-CD4 mAb. All incubations were run for 30 min at 4°C, and the frequency of $CD4^+$ T cells with each TCR V_β repertoire per total $CD4^+$ T cells was calculated by using FACSTAR and CELLQUEST software.

Preparation of Retroviral Construct with Chromatin-Specific TCR Genes and Transduction to Splenocytes. Chromatin-specific TCR V_α and V_β DNA fragments were synthesized, using PCR based on the published sequences of the nucleosome-specific T cell line derived from the lupus-prone (SWR × NZB)F_1 mouse (27, 28), as described in ref. 29. These fragments were cloned into a pMXW retroviral vector (30) and transfected into PLAT-E packaging cell lines (31) by using FuGENE6 transfection reagent (Roche Diagnostics). The viral supernatant of transfected cells were placed on fibronectin-coated 24-well plates, and total spleen cells from 2-month-old (NZB × NZW)F_1 mice prestimulated for 48 h with Con A (10 μg/ml) and interleukin 2 (50 ng/ml) were added to the wells (1×10^6 cells per well). Cells were cultured further for 36 h to allow infection to occur.

Purification and Functional Analysis of Dendritic Cells (DCs). Spleen cells were treated with collagenase type IV (Sigma) and DNase I, and $CD11c^+$ cells were positively collected by passing spleen cells twice through MACS CD11c microbeads and magnetic separation columns. The purity (85% in average) of DCs was determined by flow cytometry with anti-CD11c-biotin, followed by streptavidin-phycoerythrin.

To analyze the potential of chromatin presentation, $CD4^+$ T cells were purified by negative selection, using MACS microbeads with anti-CD19, -CD11c, and -CD8 mAbs 24 h postinfection, and 2×10^4 cells per well of T cells were cocultured with 1×10^5 cells per well of irradiated $CD11c^+$ DCs in 96-well flat-bottom plates with 1 μg/ml chromatin. After 24 h of culture, the cells were pulse-labeled with 1 μCi (1 Ci = 37 GBq) of [^{3}H]thymidine per well (NEN) for 15 h, and the [^{3}H]thymidine incorporation was determined.